Cell Death and Differentiation (2013) 20, 686–697

www.nature.com/cdd

Open

# $IF_1$ limits the apoptotic-signalling cascade by preventing mitochondrial remodelling

D Faccenda[1,4], CH Tan[2,4], A Seraphim[2], MR Duchen*[,2] and M Campanella*[,1,2,3]

**Mitochondrial structure has a central role both in energy conversion and in the regulation of cell death. We have previously shown that $IF_1$ protects cells from necrotic cell death and supports cristae structure by promoting the oligomerisation of the $F_1F_o$-ATPsynthase. As $IF_1$ is upregulated in a large proportion of human cancers, we have here explored its contribution to the progression of apoptosis and report that an increased expression of $IF_1$, relative to the $F_1F_o$-ATPsynthase, protects cells from apoptotic death. We show that $IF_1$ expression serves as a checkpoint for the release of Cytochrome *c* (Cyt *c*) and hence the completion of the apoptotic program. We show that the progression of apoptosis engages an amplification pathway mediated by: (i) Cyt *c*-dependent release of ER $Ca^{2+}$, (ii) $Ca^{2+}$-dependent recruitment of the GTPase Dynamin-related protein 1 (Drp1), (iii) Bax insertion into the outer mitochondrial membrane and (iv) further release of Cyt *c*. This pathway is accelerated by suppression of $IF_1$ and delayed by its overexpression. $IF_1$ overexpression is associated with the preservation of mitochondrial morphology and ultrastructure, consistent with a central role for $IF_1$ as a determinant of the inner membrane architecture and with the role of mitochondrial ultrastructure in the regulation of Cyt *c* release. These data suggest that $IF_1$ is an antiapoptotic and potentially tumorigenic factor and may be a valuable predictor of responsiveness to chemotherapy.**
*Cell Death and Differentiation* (2013) **20,** 686–697; doi:10.1038/cdd.2012.163; published online 25 January 2013

The efficiency of the intrinsic pathway of apoptosis[1] depends on the release of mitochondrial pro-apoptotic proteins (e.g., Cytochrome *c* (Cyt *c*)) into the cytosol, where they trigger the caspase-dependent execution of the cell.[2] Other mitochondria-associated events are: (a) changes in electron transport,[3] (b) loss of transmembrane potential ($\Delta\Psi_m$),[4] (c) $Ca^{2+}$ overload[5] and (d) re-organization of mitochondrial ultrastructure.[6,7]

The regulatory pathways that govern the dynamics of mitochondrial fusion/fission events are the object of general interest for their critical role in both cell physiology and pathology. Their relevance in apoptosis is also widely acknowledged.[8,9] Alterations in ultrastructure occur in numerous diseases and are also a feature of apoptosis. The narrow tubular junctions that connect mitochondrial cristae to the inner boundary membrane support core functions such as: (i) creating gradients of small molecules (adenosine diphosphate),[10] (ii) ions' homeostasis (e.g. $Ca^{2+}$)[11] and (iii) segregation of the respiratory chain complexes.[12] Cyt *c* localizes in the intermembrane space, and disruption of tubular junctions is required to support its release into the cytosol at the onset of apoptotic cell death.[13]

The endogenous inhibitor of the ATPase, $IF_1$, is a small, basic, heat-stable protein composed of 80–84 amino acids (~10 kDa) in mammals and predominantly compartmentalized inside the mitochondrial matrix.[14] $IF_1$ has the unique capacity to inhibit, through a non-competitive mechanism, the adenosine triphosphate (ATP)-hydrolysing activity of the $F_1F_o$-ATPsynthase without affecting the synthesis of ATP during oxidative phosphorylation. The protein is $\alpha$-helical along most of its length (~90 Å[15]) and at low pH (<6.7) becomes active as a dimer, making this the only condition in which its inhibitory role is exerted.[16] The dimerization of $IF_1$—which is critical for the inhibition of the $F_1F_o$-ATPsynthase—involves the *C*-terminal regions of two monomers (residues 37–84[17]), which form an antiparallel double-stranded coiled-coil unit stabilized by complementary hydrophobic interactions between the two helices.[18] By assessing the role of $IF_1$ on resting mitochondrial physiology and morphology, we recently reported a prominent effect on cristae number and alignment,[19] suggesting that $IF_1$ has a role in the regulation of mitochondrial ultrastructure.

Mitochondrial ultrastructure is governed by: (a) the mitofilin/Fcj1 complex, which is essential for cristae development;[20] (b) the pro-fusion protein Optic atrophy 1 (Opa1)[7] and (c) the dimerization of the $F_1F_o$-ATPsynthase.[21] The latter is promoted by $IF_1$, with increased density of cristae, contributing to the morphology of single mitochondria and that of the whole network.[22,23] In addition, dimerization of the

[1]Department of Comparative Biomedical Sciences, The Royal Veterinary College, University of London, London, UK; [2]Department of Cell and Developmental Biology and Consortium for Mitochondrial Research (CfMR), University College London, London, UK and [3]European Brain Research Institute (EBRI), Rome, Italy
*Corresponding author: M Campanella, Department of Comparative Biomedical Sciences, The Royal Veterinary College, University of London, Royal College Street, London NW1 0TU, UK. Tel: +020 7468 1239/Ext 5468; Fax. +020 7468 5204; E-mail: mcampanella@rvc.ac.uk
or MR Duchen, Department of Cell and Developmental Biology and Consortium for Mitochondrial Research (CfMR), University College London, Gower Street, London WC1E 6BT, UK. Tel: +44 207 679 3207; Fax: +44 207 813 0530; E-mail: m.duchen@ucl.ac.uk
[4]These authors contributed equally to this work.
**Keywords:** $IF_1$; apoptosis; mitochondria; Drp1; Cytochrome *c*; $Ca^{2+}$
**Abbreviations:** ATP, adenosine triphosphate; Cyt *c*, Cytochrome *c*; Drp1, Dynamin-related protein 1; $\Delta\Psi_m$, mitochondrial membrane potential; ER, endoplasmic reticulum; GFP, green fluorescent protein; mPTP, mitochondrial permeability transition pore; STS, Staurosporine; Tg, thapsigargin; YFP, yellow fluorescent protein
Received 29.6.12; revised 30.10.12; accepted 11.11.12; Edited by L Scorrano; published online 25.1.13

$F_1F_o$-ATPsynthase was recently shown to protect cells from starvation,[24] highlighting the importance of molecules with a role in this. Beside the outcome on mitochondrial morphology, $IF_1$ is key to the preservation of cellular ATP during hypoxia or ischemia,[19] but its outcome on pathways mediating apoptosis remains controversial. $IF_1$ expression is greatly increased in a number of human cancers,[25,26] and recently it has been proposed to interact with the canonical pro-survival pathway, NF-$\kappa$B,[27] priming an adaptive response. Even though this was explained via an $IF_1$-mediated inhibition of mitochondrial oxidative phosphorylation and a resultant increased production of ROS—an aspect which is still controversial[23]—this implies a mitochondrial downstream effect that would impinge on signaling pathways of cancer cells.

The shaping of the outer mitochondrial membrane is sustained by the pro-fission GTPase Dynamin-related protein 1 (Drp1)[28,29] and, during apoptosis, by the activity of the pro-apoptotic member of the Bcl-2 family Bax,[30,31] whose oligomerization facilitates mitochondrial outer membrane permeabilization.[32] Drp1 translocation to mitochondria is a $Ca^{2+}$-dependent process, as its activity is regulated by phosphorylation and dephosphorylation at several amino-acid residues: a rise in [$Ca^{2+}$] induces the $Ca^{2+}$/Calmodulin-dependent activation of Calmodulin kinase I alpha, which phosphorylates Drp1 at Ser600, and Calcineurin, which dephosphorylates Drp1 at Ser637. Both events are crucial to induce the translocation of Drp1 onto the outer mitochondrial membrane.[33,34] $Ca^{2+}$ *per se* contributes to apoptosis by facilitating mitochondrial fission when the organelles are overloaded with the ion.[35]

Moreover, Snyder and co-workers suggested that Cyt *c*, once released from mitochondria, binds to inositol 1,4,5-triphosphate receptors ($IP_3Rs$), promoting the release of $Ca^{2+}$ from the endoplasmic reticulum (ER) and increasing $Ca^{2+}$ accumulation into mitochondria.[36,37] This implies that proteins that limit disassembly of the mitochondrial network, cristae remodeling and release of Cyt *c* could also affect $Ca^{2+}$ signaling in apoptosis.

Our data demonstrate that $IF_1$ may modulate apoptosis by regulating mitochondrial morphology, so limiting Cyt *c* release. They support a model whereby Cyt *c* promotes ER $Ca^{2+}$ release, which leads to activation of Drp1 and recruitment of Bax to the outer mitochondrial membrane, where it permeabilises the membrane inducing further Cyt *c* release; this self-sustaining positive feedback amplification pathway may account for the all-or-none release of mitochondrial Cyt *c*.[38] $IF_1$—via modulation of the mitochondrial architecture—represents an early checkpoint in this pathway, limiting the efficient progression of the apoptotic cascade and protecting therefore the cells from the apoptotic cell death.

## Results

**$IF_1$ counteracts apoptotic remodeling of the mitochondrial structure.** The $IF_1$:$F_1F_o$-ATPsynthase expression ratio was manipulated in HeLa cells as in our previous studies,[19,23] using a blank vector as control. Cells expressing different levels of $IF_1$ were exposed to the pro-apoptotic agent Staurosporine (STS), a broad-spectrum protein kinase inhibitor[39] and, after 4 h of treatment, prepared for transmission electron microscopy analysis. The same experiment was repeated using etoposide.

As shown in Figure 1Aa, an extensive remodeling of cristae architecture following treatment with both stimuli characterized $IF_1$ knock down cells ($-IF_1$), while the shape of cristae remained intact in cells overexpressing $IF_1$ ($+IF_1$). The number of cristae per mitochondrion was quantified and plotted in Figure 1Ab.

Using the recombinant mitochondrially targeted green fluorescent protein , we then analyzed the mitochondrial network morphology (Figure 1Ba). In control cells, mitochondria were fragmented and disrupted after STS treatment. In $-IF_1$ cells the network was completely disrupted after only 4 h. However, within the same timeframe, no significant alteration was seen in $+IF_1$ cells (Figure 1Bb).

**$IF_1$ reduces apoptotic redistribution of Cyt *c*.** Subsequently, we investigated the entity of Cyt *c* release during apoptosis in control and $+/-IF_1$ cells via confocal imaging analysis. For this purpose, we transfected cells with the recombinant Cyt *c*-GFP chimera[33] and quantified Cyt *c* redistribution by measuring the ratio between its mean fluorescence values and the relative standard deviation of the fluorescence signal (see Materials and Methods; Figure 2Aa).

After only 2 h of STS treatment, 11% of control cells showed Cyt *c* redistribution, while in $+IF_1$ cells this was limited to just 3%, and suppression of Cyt *c* release remained even after 6 h of treatment. Conversely, in $-IF_1$ cells, the release of Cyt *c* was greater than control (Figure 2Aa). Values of each condition between 0 and 3 h of treatment were quantified and shown in Figure 2Ab. After 7–8 h of STS treatment, Cyt *c* release from $+IF_1$ cells increased, and there was no longer any significant difference.

$\Delta\Psi_m$ was measured simultaneously during Cyt *c*–GFP redistribution (Supplementary Figure S1a). In tetramethylrhodamine, methyl ester-loaded control and $+IF_1$ cells, this was done at intervals of 30 min over 8 h of STS treatment. $\Delta\Psi_m$ values, measured at every time point, were normalized between the initial baseline and the fully depolarized mitochondrial state, which was obtained by adding FCCP (carbonyl cyanide 4-(trifluoromethoxy)phenylhydrazone) at the end of each experiment.

We observed that Cyt *c* release occurred in tandem with mitochondrial depolarization and that the events took place simultaneously and interdependently in both the control and $+IF_1$ groups (values reported in Figures 2Ba and Bb).

Cyt *c* release and the loss of membrane potential were both significantly suppressed in $+IF_1$ cells during STS treatment (Figure 2B).

Although it remains contentious,[37] it has been suggested that the formation of the mitochondrial permeability transition pore (mPTP) may promote the loss of $\Delta\Psi_m$ and, possibly, Cyt *c* release during apoptosis;[40] the diverse incidence of the two events in the two groups of cells could be, therefore, due to differences in mPTP opening.[36] Hence, we repeated the analysis in the presence of Cyclosporine A, a pharmacological

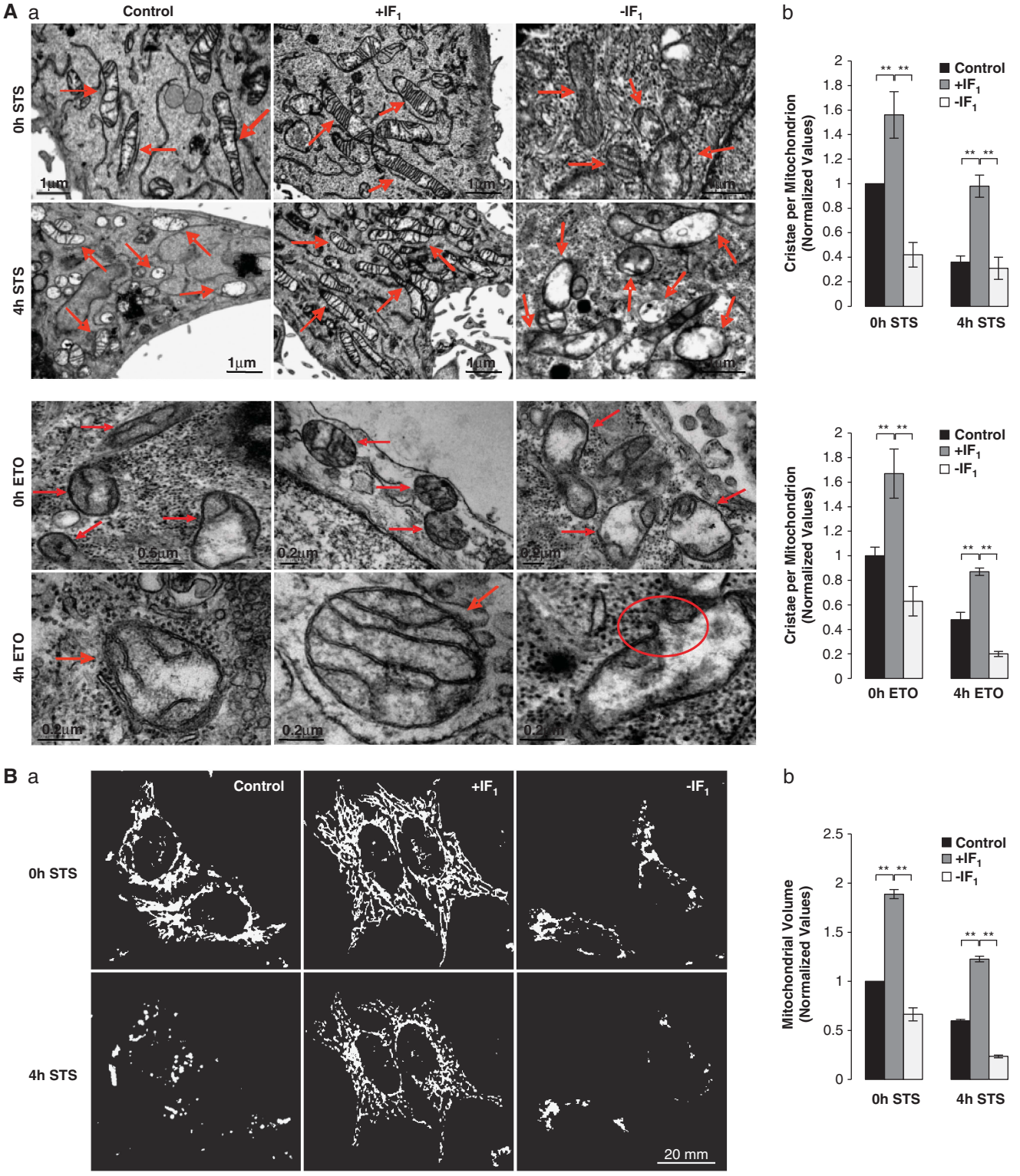


**Figure 1** Mitochondrial ultrastructure and remodeling during apoptosis depends on IF$_1$ levels. (**A**) Transmission electron microscope micrographs of HeLa cells before and after treatment with 1 $\mu$M STS and 100 $\mu$M etoposide (ETO). (a) An increased number of cristae was evident in $+$IF$_1$ cells, as highlighted by the quantification in panel (b) ($n=3$, $^*P<0.05$, $^{**}P<0.01$). (**B**) Representative confocal images of HeLa cells transfected with mtGFP before and after challenging with 1 $\mu$M STS; an overall preservation of the mitochondrial network was seen in cells overexpressing IF$_1$. Quantification of mitochondrial volume in all conditions is reported in panel (b), indicating that IF$_1$ ratio of expression is involved in the morphological adaptation of mitochondria to apoptosis ($n=3$, $^{**}P<0.01$)

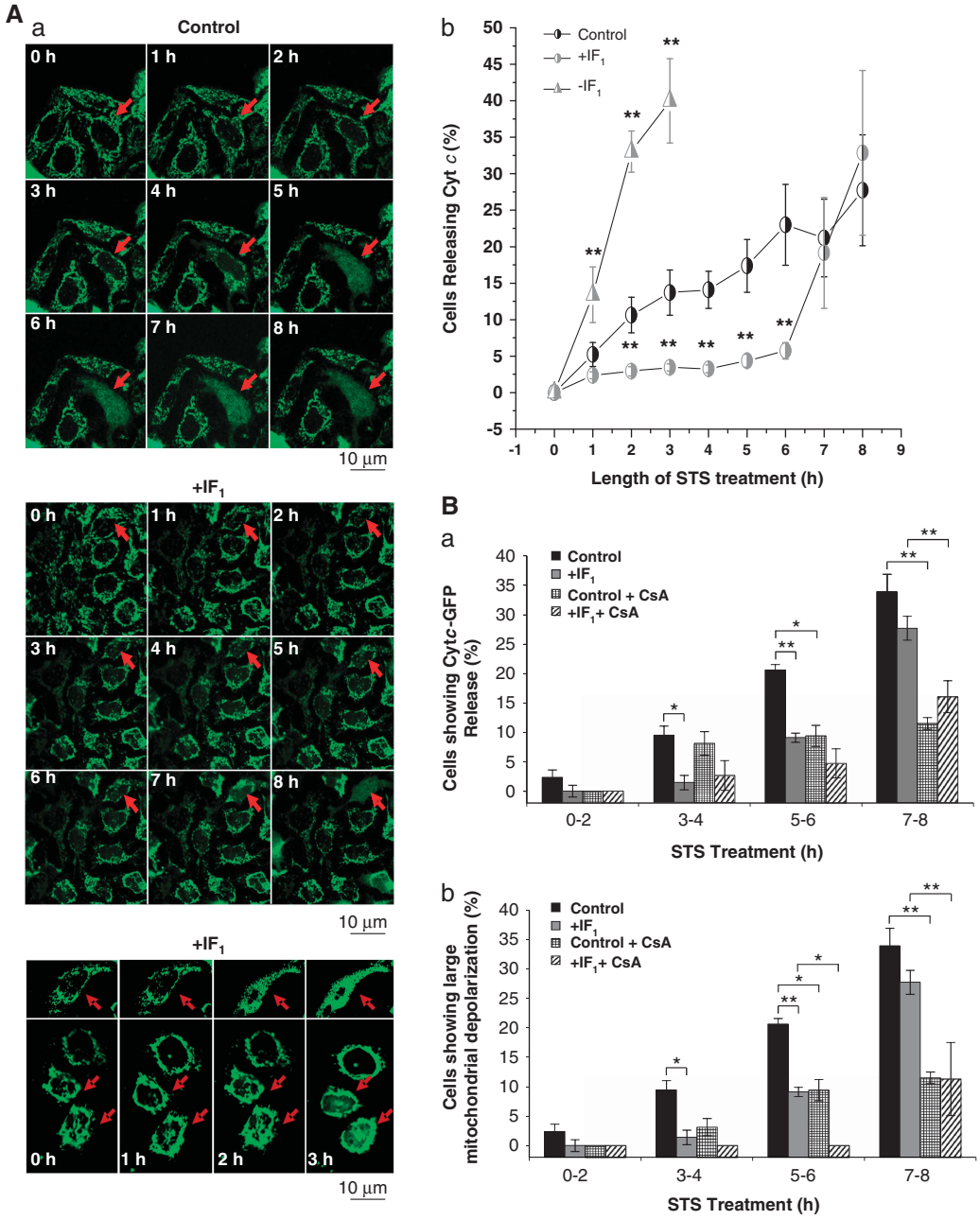


**Figure 2** $IF_1$ limits Cyt *c* release and apoptotic cell death. (**A**) Prototypical images of Cyt *c* release from mitochondria in control, $IF_1$ overexpressing or $IF_1$ knockdown HeLa cells after challenging with (a) 1 $\mu$M STS. The redistribution of Cyt *c* from the mitochondrial compartment into the cytosol was visualized cotransfecting cells with GFP-tagged Cyt *c*. The graph in panel (b) shows the percentages of control, $IF_1$ overexpressing and $IF_1$ knockdown HeLa cells releasing Cyt *c* from mitochondria during treatment with 1 $\mu$M STS. Data were acquired every hour over a period of 8 h ($n = 4$ cover slips, $^*P < 0.05$, $^{**}P < 0.01$). (**B**) Bar charts showing the percentage of control and $+IF_1$ HeLa cells with (a) redistributed Cyt *c*-GFP and (b) dissipated $\Delta\Psi_m$ at various time points of STS treatment in the absence or presence of the mPTP inhibitor Cyclosporine A (CsA). Notably, in $+IF_1$ cells a CsA-mediated inhibition of Cyt *c*-GFP release was only evident at 7–8 h, while in control cells CsA had clear effects at 5–6 h, the time point required by the drug to mediate a protective effect on $\Delta\Psi_m$ in both conditions

inhibitor of mPTP.[41] In control cells, Cyclosporine A significantly suppressed both redistribution of Cyt *c* (Figure 2Ba) and dissipation of $\Delta\Psi_m$ (Figure 2Bb) after only 5–6 h of STS treatment, while in $+IF_1$ cells the activity of Cyclosporine A was delayed, and a same effect was reached after 7–8 h. These data support a role for the mPTP in the loss of $\Delta\Psi_m$ during apoptosis.

**Apoptotic cell death is modulated by the $IF_1$:$F_1$ $F_o$-ATPsynthase ratio.** Along with the retention of Cyt *c* and $\Delta\Psi_m$ in the initial phases of apoptosis, the exposure of phosphatidylserine on the plasma membrane and the activation of Caspase 3 were also limited by $IF_1$ overexpression and facilitated by its downregulation (Figures 3Aa and Ab).

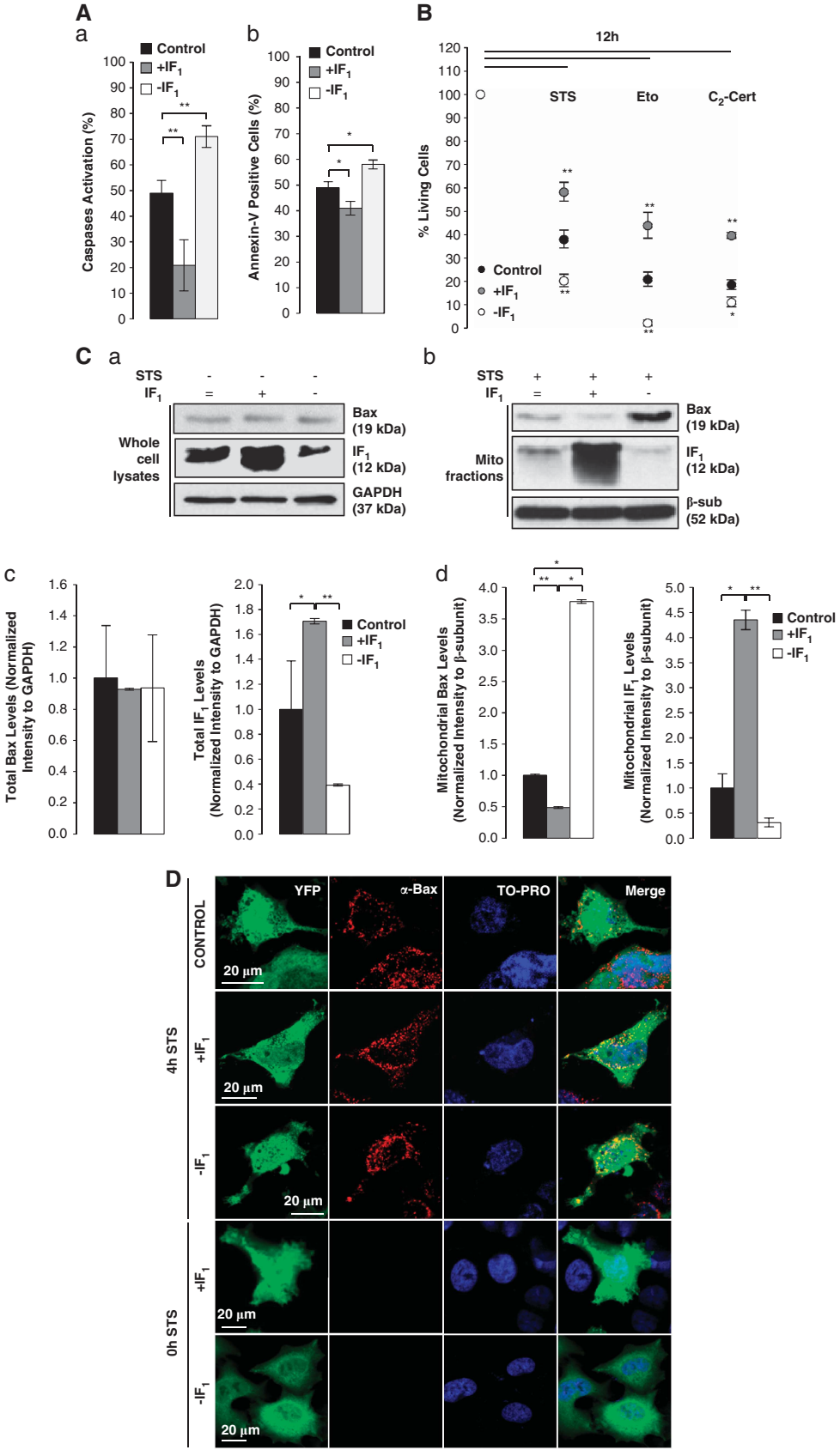
A
a
Caspases Activation (%)
Control
+IF1
-IF1
b
Annexin-V Positive Cells (%)
B
12h
% Living Cells
STS
Eto
C2-Cert
C
a
STS
IF1
Bax (19 kDa)
Whole cell lysates
IF1 (12 kDa)
GAPDH (37 kDa)
b
Mito fractions
β-sub (52 kDa)
c
Total Bax Levels (Normalized Intensity to GAPDH)
Total IF1 Levels (Normalized Intensity to GAPDH)
d
Mitochondrial Bax Levels (Normalized Intensity to β-subunit)
Mitochondrial IF1 Levels (Normalized Intensity to β-subunit)
D
YFP
α-Bax
TO-PRO
Merge
CONTROL
4h STS
0h STS
20 μm

Cell survival was measured following 12 h exposure to Staurosporine, etoposide or $C_2$-ceramide. A significant protection from apoptosis was observed in $+IF_1$ cells and the opposite in those downregulated for the gene (Figure 3B). Perhaps surprisingly, increased $IF_1$:$F_1F_o$-ATPsynthase ratio of expression was also protective from cell death triggered by the agonistic anti-CD95 antibody ($\alpha$-CD95), which activates the extrinsic pathway of apoptosis (Supplementary Figure S1bi).[42] Although not recapitulated by the deletion of the gene, as $-IF_1$ cells undergo cell death in equal measure of control, we asked whether $IF_1$ altered the expression of Caspase 8, which links the extrinsic and intrinsic pathways of apoptosis (Supplementary Figure S1bii). This analysis revealed that Caspase 8 expression was not modulated by changes in $IF_1$ expression but that in $+IF_1$ cells treatment with $\alpha$-CD95 promotes a more prominent cleavage in the p43/41 fragments, which would account for an increased activation of the pathway.

**$IF_1$ overexpression limits the activity of Bax and Drp1 on mitochondria.** During apoptosis, Bax translocates onto the MOM and, after a conformational shift with exposure of the *C*-terminus, inserts into it, facilitating the release of Cyt *c*.[43] We therefore assessed Bax expression levels in control and $+/-IF_1$ cells. Bax appeared to be evenly expressed in all the cell types at resting physiology (Figure 3Ca).

Fractions of purified mitochondria isolated after 4 h of treatment with STS were probed with an anti-Bax antibody; although almost no staining was detectable in $+IF_1$ cells, the observed band intensity in $-IF_1$ cells was much greater than control cells ($n=5$) (Figure 3Cc). In addition, this trend was also confirmed by immunocytochemical analysis (Figure 3D).

Mitochondrial outer membrane permeabilisation, effected by Bax, depends on the remodeling of membranes, for which the recruitment of Drp1 to mitochondria is required.[30] Mitochondrial fractions tested for Drp1 expression showed that downregulation of $IF_1$ facilitates the relocation of Drp1 onto mitochondria during apoptosis, as the protein was retrieved in greater amount when compared with the cytosolic fraction, whereas the opposite was seen following overexpression of $IF_1$ (Figure 4Aa). As for the analysis of Bax, we used an immunocytochemical analysis to confirm the data (Figure 4Ac).

In addition, Drp1 activation differed between mitochondria expressing diverse levels of $IF_1$, as extracts of $-IF_1$ cells were more strongly stained with the anti-pospho-Drp1(S616) antibody that recognizes the active form of the protein (Figure 4B).

These data suggest that $IF_1$ overexpression reduces Drp1 translocation to mitochondria, as well as the interdependent translocation and oligomerisation of Bax. We therefore expressed the dominant-negative mutant of Drp1 (Drp1K38A) in $+/-IF_1$ cells, and measured the percentage of living cells after 12 h incubation with STS. Under these conditions, we saw no differences between the three conditions compared with cells expressing naive levels of Drp1 (Figure 4C). The same outcome was obtained in $Drp1^{-/-}$ cells (data not shown).

**$IF_1$ limits $Ca^{2+}$ mobilization during apoptosis activation.** According to Boehning *et al*.,[36] Cyt *c* binds to $IP_3Rs$ on the adjacent ER at the beginning of apoptosis, thus enhancing $Ca^{2+}$ release, mitochondrial $Ca^{2+}$ loading and opening of the mPTP, so amplifying the release of Cyt *c*. As the redistribution of Cyt *c* and the loss of mitochondrial potential were significantly delayed in $+IF_1$ cells, we explored the potential role of $Ca^{2+}$ signaling in this pathway. Cells transfected with $IF_1$ cDNA and control cells were loaded with Fura-2, AM, treated with STS and imaged over 8 h. Alternative patterns of $[Ca^{2+}]_c$ signals were seen with varying frequencies in control and $+IF_1$ cells (Figures 5Aa and Ab). The majority of $+IF_1$ cells (85.60%) showed no change in $[Ca^{2+}]_c$ compared with $\sim$40% of control cells, in which a significant percentage showed either a progressive increase (13.09%) or spikes (46.86) in $[Ca^{2+}]_c$, which were very rarely observed in $+IF_1$ cells. $IF_1$ overexpression reduced STS-induced changes in $[Ca^{2+}]_c$, and this effect correlated with the delay in Cyt *c* release from mitochondria (as quantified in Figure 2Ab).

The differences in $[Ca^{2+}]_c$ patterns may be attributed to differences in the initial release of Cyt *c*, which may modulate ER $Ca^{2+}$ signaling so amplifying Cyt *c* release to completion. We therefore measured the ER $Ca^{2+}$ content using Thapsigargin (Tg, 500 nM) at several time points following exposure to STS. Representative traces of changes in $[Ca^{2+}]_c$ following STS treatment and Tg application are shown in Figures 5Ba and Bb. As reported in Supplementary Figure S1ciii, $[Ca^{2+}]_{ER}$ was substantially depleted in control cells compared with $+IF_1$ cells, consistently with the increased release of ER $Ca^{2+}$ seen in control cells.

Remarkably, as a chance observation, we noted that STS altered the capacitative $Ca^{2+}$ influx in both control and $+IF_1$ cells; in fact, while in untreated cells $[Ca^{2+}]_c$ remained elevated after addition of Tg (Figure 5Ba), it decreased to

**Figure 3** $IF_1/F_1F_o$-ATPsynthase ratio of expression regulates cell response to apoptosis modulating the activity of Bax. (**A**) Bar charts displaying the percentage of control and $IF_1$ up/downregulated HeLa cells with (a) caspase activation and (b) positive Annexin-V staining after 14 h treatment with 1 $\mu$M STS. Remarkably, in $+IF_1$ cells caspase activation and exposure of phosphatidylserine to the extracellular environment were lower than in control cells, while an opposite situation was seen in $-IF_1$ cells (*$P<0.05$, **$P<0.01$). (**B**) Chart reporting the percentage of living cells after 12 h treatment with 1 $\mu$M STS, 20 $\mu$M $C_2$-Cer or 100 $\mu$M etoposide (ETO) in control, $+IF_1$ and $-IF_1$ HeLa cells. An augmented resistance to all apoptotic stimuli was evident in $+IF_1$, cells, whereas $-$IF1 cells showed an opposite effect ($n=3$, *$P<0.05$, **$P<0.01$). (**C**) (a and b) Western blot analysis of cells modulated for $IF_1$ expression, showing that total cellular levels of Bax were not affected by the expression levels of $IF_1$. Band densities have been quantified and normalized to GAPDH (glyceraldehyde 3-phosphate dehydrogenase). The western blot in panel (c) shows instead that, during STS-induced apoptosis (4 h treatment with 1 $\mu$M STS), Bax accumulation was limited in cells overexpressing $IF_1$. After treatment, cells devoid of $IF_1$ exhibited higher levels of Bax in the mitochondrial fraction, indicating an increased mitochondrial recruitment during apoptosis (band densities, quantified and normalized to the $\beta$-chain of $F_1F_o$-ATPsynthase, are reported in panel (d); $n=6$; *$P<0.05$, **$P<0.01$). (**D**) Representative immunocytochemistry images showing Bax translocation to mitochondria in control, $+IF_1$ and $-IF_1$ HeLa cells after 4 h treatment with 1 $\mu$M STS

basal levels in STS-treated cells (Figure 5Bb). A similar pattern occurred up to 6 h of STS treatment, as reported in Supplementary Figures S1ci and cii.

Uptake of $Ca^{2+}$ by mitochondria was then measured using Rhod-2, AM (Figure 5Ca). After 2 h of STS treatment, mitochondria of $+IF_1$ cells showed no significant increase in

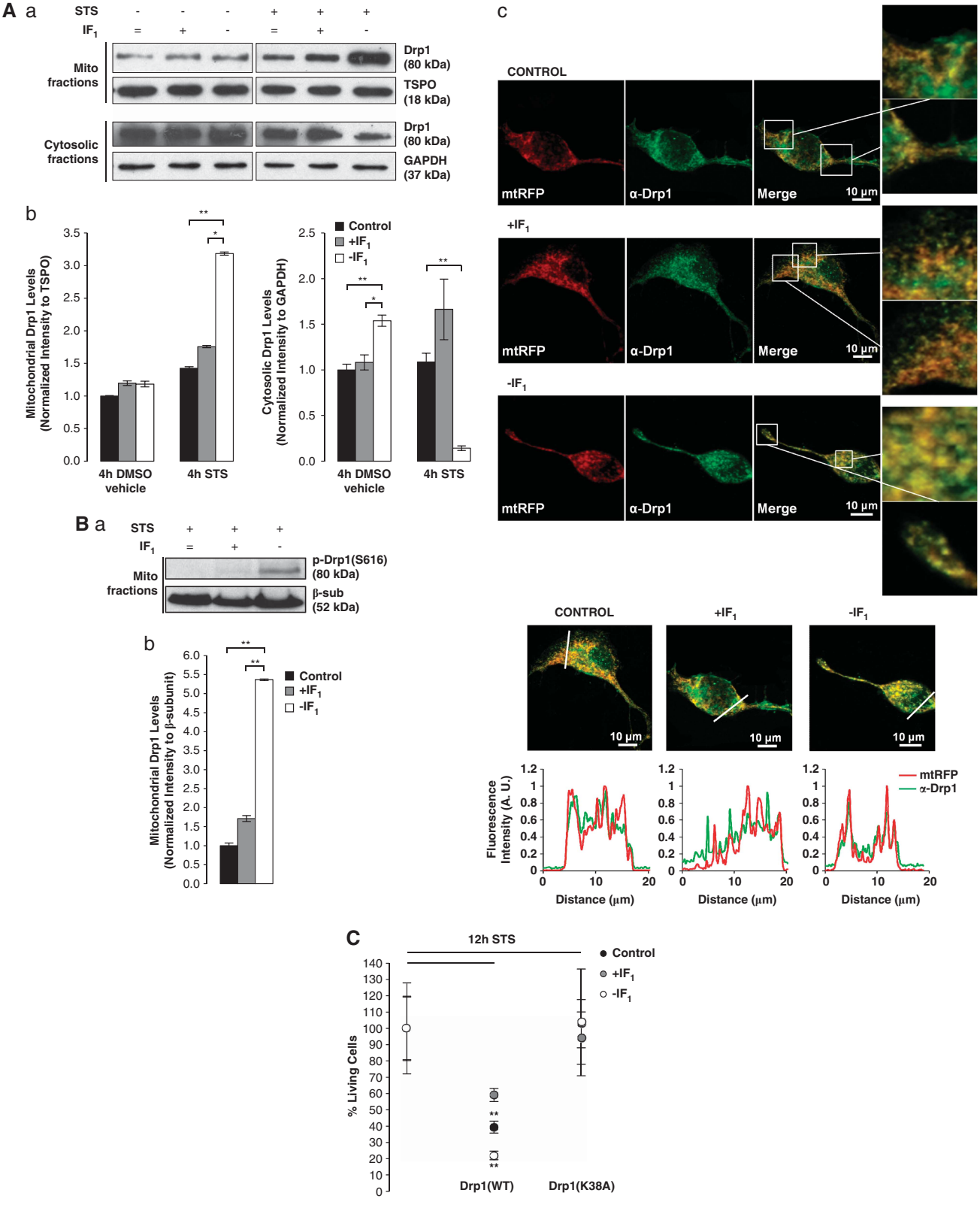

$Ca^{2+}$ content, while this was elevated in control cells. Quantified data are plotted in Figure 5Cb.

In cells overexpressing $IF_1$, the limited mobilization of $Ca^{2+}$ also reduced the activity of the serine/threonine protein phosphatase Calcineurin. Activity of Calcineurin, the $Ca^{2+}$-dependent activator of Drp1, was reduced after treatment with STS in $+IF_1$ cells, with an opposite result in $-IF_1$ cells (Figure 5D).

The hierarchy of the events we attribute to $IF_1$ is presented as a cartoon in Figure 5E.

## Discussion

Mitochondrial fragmentation and cristae remodeling augment Cyt *c* release to completion within minutes during apoptosis.[2,38] Proteins involved in the regulation of mitochondrial dynamics have an active part in this process, opposing or facilitating the structural changes of the organelle.[44] For example, Opa1 maintains the shape of cristae, reduces the mobilization of Cyt *c* and delays cell death,[45] while Drp1, which is essential for mitochondrial fission, has an opposite effect, by sustaining the oligomerization of Bax.[30] Here, we demonstrate that $IF_1$ also contributes to the structural rearrangement of mitochondria during apoptosis, modifying the mobilization of Cyt *c* and so altering the downstream cascade of events.

Our data suggest that $IF_1$ overexpression limits mitochondrial release of Cyt *c*, so that the downstream events that amplify Cyt *c* release and complete the apoptotic program are delayed. Overexpression of $IF_1$ preserved cristae morphology (Figure 1) and reduced Cyt *c* release (Figure 2), $Ca^{2+}$ signaling (Figure 5), Drp1 activation (Figure 4) and Bax oligomerisation (Figure 3) for 7 h after STS treatment (Figures 1,2, and 4), also delaying: (i) caspase activation, (ii) phosphatidylserine translocation and (iii) cell death (Figure 3). The opposite was seen in cells in which $IF_1$ expression was suppressed, as just 2 h of treatment with STS were sufficient to produce an almost complete re-distribution of Cyt *c* (Figure 2Aa).

Interestingly, $IF_1$ was also protective when apoptosis was activated via the CD95/APO-1/Fas signaling pathway (Supplementary Figure S1bi). Because the Caspase 8 cascade, via cleavage of BID,[46] merges on the mitochondrial pathway. The increased activation retrievable in +IF1 cells in which apoptosis is delayed, does imply a prominent mitochondria mediated effect.

Mitochondria were not immune from the apoptotic-associated events when $IF_1$ was overexpressed, as both migration of Cyt *c* and dissipation of $\Delta\Psi_m$ did take place, even if at a later stage—after 7 h of incubation with STS. Even though at this time point the events on which protection by $IF_1$ is primed in the initial phases are statistically normalized, it has to be noted that (a) the trend toward delay of Cyt *c* release and $\Delta\Psi_m$ dissipation remains similar to those statistically proven at 3–4 h and (b) modulation of both events occurring earlier in time are associated with a significant protection from cell death when $IF_1$ is overexpressed (Figure 3).

Notably, such a regulation of apoptosis efficiency by $IF_1$ appears independent of the canonical action of the protein as an inhibitor of the reverse mode of the $F_1F_o$-ATPsynthase.[47] One might predict that apoptosis itself should predispose to a similar scenario, with reversal of the ATP synthase and accelerated ATP consumption so that $\Delta\Psi_m$ dissipation would occur faster in $+IF_1$ cells. This was not the case: even though $IF_1$ dimers were still present after STS treatment with a greater degree (Supplementary Figure S1d), these did not influence $\Delta\Psi_m$ that dissipated concomitantly with the release of Cyt *c* and, consequently, with the permeabilisation of mitochondria.

The regulation of apoptosis by $IF_1$ embeds other elements of the process, such as (a) the multidomain protein Bax and (b) Drp1. Cuezva and co-workers have proposed that $IF_1$ overexpression influences proteins of the Bcl-2 family by increasing the expression of Bcl-XL.[27] For this reason, we explored whether expression of Bax was also altered, but we found no changes in its expression despite alternative degrees of $IF_1$ expression. We only observed changes during active apoptosis and just in the mitochondrial localization of the pro-apoptotic molecule, an event that was almost absent in $IF_1$-overexpressing cells (Figures 3Cc and Cd). Even though such an effect may be due to the increment of the anti-apoptotic counterparts of the same family—hence in line with the findings of an increased presence of BcL-XL[48,49]—other events may still modify the anchoring capacity of Bax, and the translocation/activation of the pro-fission protein Drp1 is one of these (Figures 4A and B).[30] The effects of $IF_1$ on mitochondrial morphology (Figure 1) primed the analysis based on the recently proposed model of Martinou and colleagues, in which the degree of mitochondrial Drp1 is instrumental for promoting Bax-contributed remodeling of the membranes.[30] This explains our findings whereby in $-IF_1$ cells a dramatic increase in mitochondrial translocation of Drp1 is followed by activation (Figure 4B).

Thus $IF_1$, although intramitochondrially localized, can reach out and affect mediators of apoptosis localized in the cytosol (e.g., Drp1), as confirmed by the fact that modulation of $IF_1$ expression was ineffective in altering the apoptotic response when cells expressed the dominant-negative mutant of Drp1 (Figure 4D). A similar scenario—with different actors—was also proposed in a previous relevant work, with a role for NF-$\kappa$B as the underlying proliferative pathway via which $IF_1$ exploited its anti-apoptotic and tumorigenic role.[27] As this was linked to concomitant changes in mitochondrial respiration

**Figure 4** Drp1 activation and relocation on mitochondria depends on $IF_1$. (**A**) (a and b) Western blot (WB) analysis indicating that Drp1 recruitment to mitochondria during apoptosis (still 4 h treatment with 1 $\mu$M STS) was increased after knocking down $IF_1$ (band density quantification for mitochondrial and cytosolic Drp1 is reported below; $n=4$, $^*P<0.05$, $^{**}P<0.01$). (c) Immunocytochemical analysis of Drp1 recruitment on mitochondria—still at 4 h treatment with STS. In cells devoid of $IF_1$, Drp1 colocalized on mitochondria at higher levels, as highlighted in the representative images reported and relative intensity. (**B**) During apoptosis, (a) activated Drp1 (phosphorylated at Ser616) was detectable in WB analysis in the mitochondrial fraction of $-IF_1$ cells (with relative band density quantification reported in panel (b); $n=3$, $^*P<0.05$, $^{**}P<0.01$). (**C**) Chart reporting the percentage of living cells after 12 h treatment with 1 $\mu$M STS in control, $+IF_1$ and $-IF_1$ HeLa cells co-transfected with the enzymatically inactive mutant Drp1K38A cDNA. The Drp1-dependent effect of $IF_1$ is revealed by the fact that, when Drp1 was not active, all cell populations were protected from apoptosis, with no detectable differences in the percentage of living cells after STS treatment ($n=2$, $^*P<0.05$, $^{**}P<0.01$)

that we have not observed under any condition, we remain unsure how to reconcile these different data sets.

It is possible to speculate that reduced translocation of Drp1 to mitochondria depends on alterations in the ratio of hFis-1[50] per mitochondrion—considering the organelle's elongation after Atpif1 upregulation—however, because at resting physiology we find the same amount of mitochondrial Drp1 regardless the $IF_1$:$F_1F_o$-ATPsynthase ratio, this may be mediated by upstream $Ca^{2+}$-dependent events.

It has been proposed that Cyt *c*, once released from the mitochondria into the cytosol, binds to $IP_3$Rs, inducing ER $Ca^{2+}$ release[37] and mitochondrial $Ca^{2+}$ overload, which promotes swelling and opening of the mPTP.[51] In addition, Drp1 dephosphorylation by Calcineurin, and its subsequent translocation to mitochondria, is also mediated by $Ca^{2+}$. As $IF_1$ delayed the release of Cyt *c* and suppressed ER $Ca^{2+}$ mobilization in both cytosolic and mitochondrial compartments, we explored the activity of Calcineurin as the logical link between $Ca^{2+}$ and Drp1.[33,52] Consistent with this model, in $+IF_1$ cells activation of the protein phosphatase was much reduced.

Doubts remain about whether the elongated shape of mitochondria affects the contact sites between ER and mitochondria and, ultimately, the $Ca^{2+}$-buffering capacity of mitochondria; however, the kinetics of cytosolic [$Ca^{2+}$] during STS treatment being equal in both the control and $+IF_1$ cells after Tg challenge, we ruled out this option.

Thus, we propose that, besides its role in ischemia,[19] $IF_1$ also protects from apoptotic cell death, primarily by influencing mitochondrial ultrastructure and membrane remodeling.[19,23]

Our data support a model of apoptosis that involves a cascade of actions, which will serve as an amplification mechanism to ensure the rapid, complete and efficient release of all mitochondrial Cyt *c* within a short time frame. Some elements of the scheme, outlined in Figure 5, have been controversial, but it turns out that increased expression of $IF_1$ proves an invaluable tool to interrupt this cascade, revealing the importance of downstream processes.It is therefore tempting to propose that the increased expression of $IF_1$ described in human cancers may point to a tumorigenic role for $IF_1$, given its antiapoptotic action; assaying $IF_1$ levels in cancer biopsies may thus provide a useful prognostic indicator for chemotherapy responsivity.

## Materials and Methods

Experiments were carried out in Human Cervical Adenocarcinoma cells (HeLa), wild-type and $Drp1^{-/-}$ mouse embryonic fibroblasts. Cells were transfected as explained previously.[19]

**Investigating mitochondrial morphology.** Confocal images of mitochondrially targeted GFP-positive cells were acquired as previously described.[23] For electron micrograph analysis, transfected cells were grown on gridded cover slips and 36 h after transfection identified by fluorescence microscopy and their localization marked. Cells were processed as described in precedence[19] and images acquired with a 2 JEOL 1010 transmission electron microscope (Jeol Ltd., Tokio, Japan). Acquired images were analyzed using Image J (National Institutes of Health, Bethesda, MD, USA) and 'Lucida' (Kinetic Imaging, Andor Technology plc., Belfast, UK) to define the number of cristae per mitochondrion.

**Cell death analysis.** At a confluence of ~50%, cells cultured on Ø 22 mm borosilicate cover slips were transfected with $IF_1$ cDNA, $IF_1$ siRNA or yellow fluorescent protein (YFP) cDNA (as a control). After 36 h of transfection, cells were incubated for 12 h at 37 °C, 5% $CO_2$ with one of the following apoptosis inducers: 1 $\mu$M STS (Calbiochem 569 397; Merck Millipore, Billerica, MA, USA), 100 $\mu$M etoposide (Sigma-Aldrich Co, St. Louis, MO, USA), 20 $\mu$M $C_2$-ceramide or 1 $\mu$g/ml anti-CD95 (Clone CH11) Ab (No. 05-201, Millipore, Merck Millipore). After that time, a period established to achieve significant death but leaving a reasonable number of surviving cells for adequate data collection, cells were washed with recording medium and cover slips were assembled into a chamber for confocal imaging. Annexin V and poly-caspases analysis were carried out according to the manufacturers' instructions (BD Pharmingen TM 550 911; BD Biosciences, San Jose, CA, USA), Poly-Caspases FLICA kit, category No. 92, IT) with a Zeiss LSM confocal laser scanning microscope (Carl Zeiss Group, Oberkochen, Germany) (inverted configuration on an Axiovert 200), using a 'Fluar' ×40/1.30 oil immersion objective. Images were analyzed using the LSM Image Browser software (Carl Zeiss Group).

**Evaluation of Cyt *c* redistribution.** Cyt *c* release was followed using the Cyt *c*-GFP fusion protein. Cells were seeded on Ø 22 mm borosilicate cover slips and, when ~50% confluent, cotransfected with either $IF_1$ and Cyt *c*-GFP cDNAs ($+IF_1$ cells), IF1 siRNA (Hs_ATPIF1_2; SI00308112, Qiagen, Hilden, Germany) and Cyt *c*-GFP cDNA ($-IF_1$ cells) or an empty vector and Cyt *c*-GFP cDNA (control cells). Thirty-six hours after transfection, each cover slip was mounted into a chamber for live-cell imaging and inserted into the thermostatted chamber of a Zeiss LSM 510 confocal laser scanning microscope (inverted configuration on an Axiovert 200 frame), with temperature constantly set at 37 °C. Images were acquired using a 'Fluar' ×40/1.30 oil immersion objective and an Argon laser (488 nm line; 1% laser power) to excite GFP, which fluorescence was captured through the HFT 488 dichroic mirror with BP 500/530 band-pass filter. At the start of each experiment, one image was captured for baseline measurements; then, 1 $\mu$M STS was added to recoding medium and images were hourly acquired until end (8 h after STS addition for $+IF_1$ cells, 4 h for $-IF_1$ cells). Analysis was

**Figure 5** $IF_1$ overexpression counteracts $Ca^{2+}$ mobilization and Calcineurin (CaN) activation during apoptosis. (**A**) (a) Traces of control and $+IF_1$ HeLa cells loaded with 5 $\mu$M Fura-2, AM, treated with 1 $\mu$M STS and imaged for 8 h, monitoring changes in cytosolic $Ca^{2+}$ levels. Three types of cytosolic [$Ca^{2+}$] patterns were observed. Data summarized in panel (b) illustrate that a significantly higher percentage of $+IF_1$ cells showed no changes in cytosolic [$Ca^{2+}$] levels as compared with control cells. Conversely, a higher percentage of control cells showed rises and spike-like increases in cytosolic [$Ca^{2+}$] during STS treatment. ($n=3$ cover slips, 15–29 cells per cover slip, $^*P<0.05$). (**B**) Representative traces of changes in $[Ca^{2+}]_c$ in control and $+IF_1$ HeLa cells exposed to 1 $\mu$M STS and then challenged with 500 nM Tg to specifically inhibit the activity of sarco/ER $Ca^{2+}$-ATPases. The release of $Ca^{2+}$ in the cytosol was measured to infer ER $Ca^{2+}$ content. In the absence of (a) STS, ER $Ca^{2+}$ content was not significantly different in control and $+IF_1$ cells; (b) after 2 h of STS treatment, $[Ca^{2+}]_{ER}$ content was instead greatly depleted in control cells, but better maintained in $+IF_1$ cells. (**C**) Representative (a) images and (b) kinetics of mitochondrial $Ca^{2+}$ handling monitored with Rhod-2, AM during treatment with 1 $\mu$M STS in control and $+IF_1$ HeLa cells. Although control cells exhibited a rise in $[Ca^{2+}]_m$ after challenging with STS, in $+IF_1$ cells mitochondrial $Ca^{2+}$ levels were stably maintained (normalized signals; 1 h, Control: 1.34 ± 0,39; $+IF_1$: 2.23 ± 0.49, 2 h, Control: 2.21 ± 0.07; $+IF_1$: 1.28 ± 0.13; 3 h, Control: 1.18 ± 0.05; $+IF_1$: 0.92 ± 0.08; $n=4$, 10 cells per condition, $^*P<0.05$). (**D**) Histogram reporting the enzymatic activity of CaN in control, $+IF_1$ and $-IF_1$ cells. Cells were treated for 4 h with STS to induce apoptosis or with DMSO as a control. The activity of CaN has been measured and reported as nmol of $PO_4$ released (values are normalized to control). Notably, in $-IF_1$ cells this value was higher at resting conditions and after triggering apoptosis, indicating a higher activation of CaN, while $IF_1$ overexpression inhibits this event ($^*P<0.05$; $^{**}P<0.01$). (**E**) Model for $IF_1$ functional role in apoptosis: $IF_1$ preserves the inner mitochondrial membrane structure by increasing the cristae stability,[1] reducing the release of Cyt $c$[2] and hence avoiding the Cyt *c*-induced mobilization of ER-stored $Ca^{2+}$.[3] This limits CaN activity[4a,b] and hence Drp1 recruitment/activation on mitochondria, also hindering the function of Bax.[5] The delayed massive mitochondrial release of Cyt *c* prevents the formation of the apoptosome into the cytosol and the execution of apoptosis[6]

carried out using AQM Advance 6 software (Andor, Belfast, UK) to obtain ratios of the S.D. of the green-fluorescent signal relative to the mean (S.D./Mean) for the Cyt *c*–GFP fluorescence emission; this gives a quantifiable measure of Cyt *c* redistribution in each region of interest analyzed. In brief, when the Cyt *c*-GFP chimeric protein is localized into mitochondria, the S.D. is high because there are bright pixels (corresponding to mitochondria) interspersed with black pixels (corresponding to cytoplasm). Once Cyt *c*–GFP redistributes through the cytosol, the S.D. falls as the signal is evenly distributed throughout the cell; this needs to be normalized with respect to the mean signal simply because S.D. is also a function of the overall intensity. The S.D./Mean values of Cyt *c*–GFP signal in all the analyzed cells were binned to explore the distribution. Changes in distribution of the ratio following treatment with STS from time 0–4 h were plotted for control and $+IF_1$ cells. The distribution for control cells displayed a leftward shift from time 0–4 h after STS treatment compared with that of $+IF_1$ cells, showing that more control than $+IF_1$ cells had undergone Cyt *c* redistribution. Control cells analyzed at 4 h from STS addition were expected to consist of two populations, one showing Cyt *c* release and the other one without. Indeed, the distribution plot for control cells at 4 h was fitted well by the sum of two Gaussian distributions representing the two sub-populations of cells. An intersection point between the two Gaussian populations was demarcated and threshold S.D./Mean values of the Cyt *c*-GFP signal were set to define the two populations. Cells with S.D./Mean ratios of $<0.6$ were defined as those that showed Cyt *c* redistribution, and cells with S.D./Mean $>0.7$ were considered as those that did not show Cyt *c* release from mitochondria.

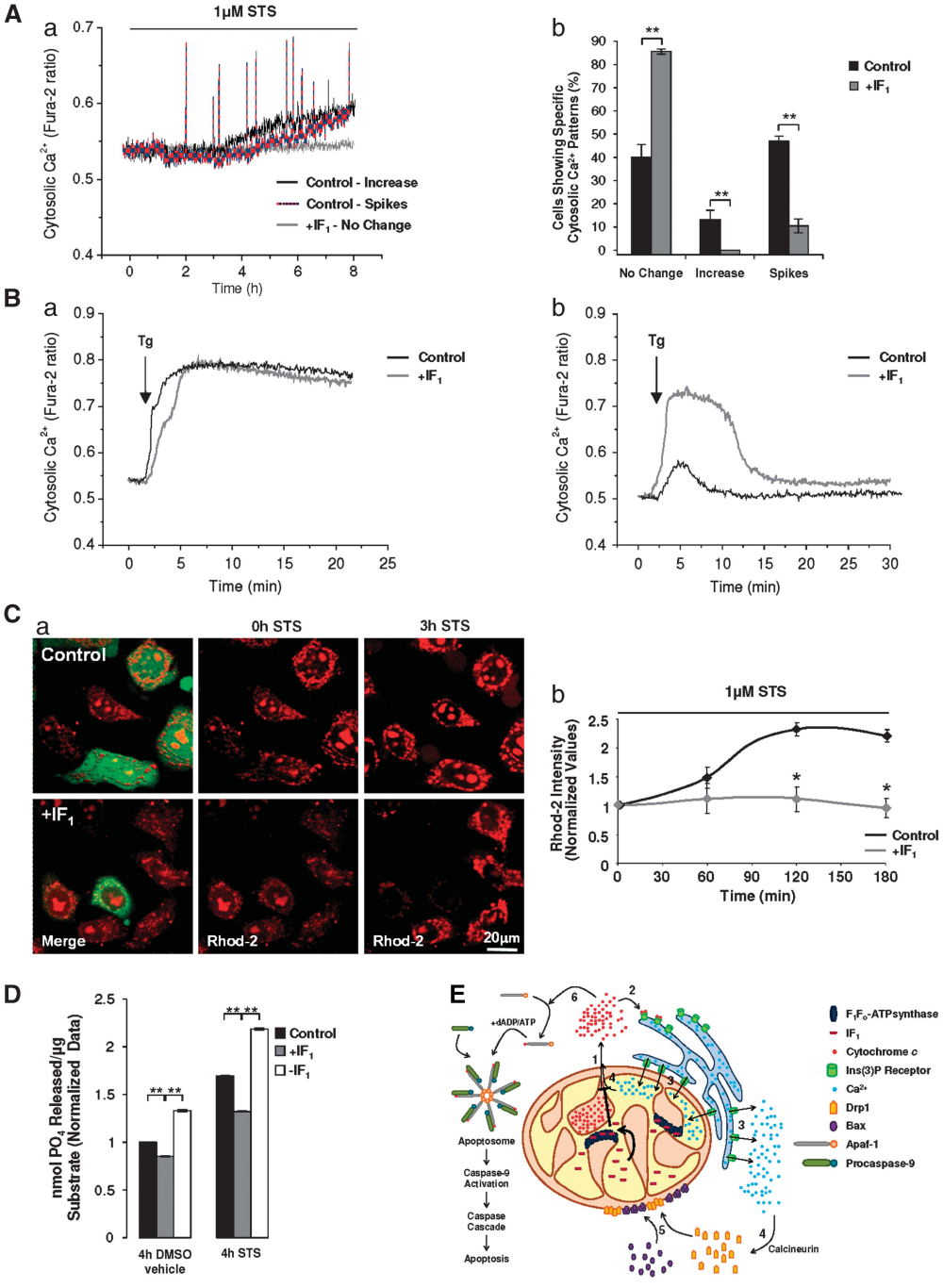

**$Ca^{2+}$ measurements.** The red-fluorescent ratiometric $Ca^{2+}$ indicator Fura-2, AM was used to measure cytosolic-free $Ca^{2+}$ levels in live cells. At low concentrations of the indicator, 340/380 nm excitation ratio allows accurate measurements of the intracellular concentration of the divalent cation. Once ~50% confluent, cells seeded on Ø 22 mm borosilicate cover slips were transfected with either IF$_1$-YFP cDNA or YFP cDNA. After 36 h of transfection, cells were loaded with 5 $\mu$M Fura-2, AM and in presence of 0.005% (w/v) pluronic acid (30 min incubation at RT—~21 °C). The loading solution was then removed, and cells were washed twice with modified Hanks' Buffered Salt Solution (HBSS 138 mM NaCl, 5.4 mM KCl, 0.25 mM $Na_2HPO_4$, 0.44 mM $KH_2PO_4$, 1.3 mM $CaCl_2$, 1.0 mM $MgSO_4$, 4.2 mM $NaHCO_3$, pH 7.4). Each cover slip of cells was assembled into a purpose-built chamber, a fresh aliquot of modified HBSS with or without 1 $\mu$M STS was added to the cells and placed on the stage of a Leica TCS SP5 II confocal laser scanning microscope (Leica Microsystems GmbH, Wetzlar, Germany). Temperature inside the environmental chamber of the microscope was constantly maintained at 37 °C. Images were acquired for 8 h using a HCX PL APO 40 × /1.25-0.75 oil immersion CS objective and collecting Fura-2 emission at 505 nm in the ratio mode with excitation of the dye at 340 and 380 nm light (using an UV laser, a 400 long pass dichroic mirror and a 510/540 band pass filter). Settings were adjusted to minimize phototoxicity. Acquired images were analyzed with the AQM Advance 6 software making a 340/380 nm.

For experiments measuring ER $Ca^{2+}$ content, cells loaded with Fura-2, AM and treated with 1 $\mu$M STS for the required number of hours were challenged with Tg, a sarcoplasmic reticulum $Ca^{2+}$-ATPase inhibitor, to prevent $Ca^{2+}$ reuptake into the ER.

Mitochondrial $Ca^{2+}$ levels were analyzed with the red-fluorescent $Ca^{2+}$ indicator Rhod-2, AM. Cells were seeded on Ø 22 mm borosilicate cover slips and transfected with either IF$_1$-YFP cDNA or YFP cDNA when ~50% confluent. After 36 h, cells were loaded with 5 $\mu$M Rhod-2 in the presence of 0.05% (w/v) pluronic acid in modified HBSS (45 min incubation at 37 °C, 5% CO2). After four washes with modified HBSS to remove excess dye, cover slips were assembled into a live-cell imaging chamber and an aliquot of modified HBSS with 1 $\mu$M STS (or DMSO (dimethyl sulfoxide) vehicle as a control) was added. Cover slips were then seeded into the thermostatted chamber of a Zeiss LSM 510 Confocal Laser Scanning Microscope (inverted configuration on an Axiovert 200 frame) and cells were imaged using a 'Fluar' 40 × /1.30 oil immersion objective and a green Helium-Neon laser (543 nm line; 1% laser power) with a BP 565/615 band-pass filter. Settings were chosen to reduce photobleaching of the fluorophore and the pinhole set to give an optical slice of ~2 $\mu$m. Acquisitions were taken every 30 min to obtain a time course of mitochondrial $Ca^{2+}$. Images were analyzed with the LSM Image Browser.

**Western blotting.** At a confluence of ~50%, cells cultured on 100 mm Petri dishes were transfected with either IF$_1$ cDNA, IF$_1$ siRNA or YFP cDNA (as a control). After 36 h of transfection, cells were incubated with 1 $\mu$M STS supplemented recording medium (4 h incubation at 37 °C, 5% CO2) to induce apoptosis. Subcellular fractionation was then executed. Cells were mechanically harvested in 5 ml of ice-cold PBS with a cell scraper and centrifuged to pellet cells. Pellets were resuspended in 1 ml of isotonic buffer supplemented with protease inhibitors, and cells were lysed by homogenization with 60 strokes using a Dounce homogenizer (Sigma-Aldrich Co.). Homogenates were centrifuged for 10 min at 600 × *g* at 4 °C; pellets (nuclei and debris) were discarded and supernatants were centrifuged for 10 min at 13 000 × *g* at 4 °C. Pellets (mitochondria) were dissolved in 1 ml isotonic buffer and centrifuged as above; while supernatants were centrifuged at 100 000 × *g*, and the resulting supernatants were designated as cytosolic fractions. Mitochondria were then lysed by incubating mitochondrial pellets with *ad hoc* lysis buffer (50 mM Tris-HCl pH 7.4, 50 mM NaCl, 1% Triton X-100, 1 mM EDTA, 1 mM EGTA, 5 mM $MgCl_2$) supplemented with protease inhibitors for 30 min at 4 °C on rotating platform, followed by 30 min centrifugation at 14 000r.p.m. in a refrigerated benchtop centrifuge; supernatants were designated as mitochondrial fractions. Proteins' concentration was analyzed with Pierce BCA Protein Assay Kit (Thermo Scientific Inc., Rockford, IL, USA).

Western blotting was carried out as previously described, using antibodies against IF$_1$ (1 : 1000, a generous gift from Prof. Sir John Walker), Bax (N-20) (1 : 100; Sc-493, Santa Cruz Biotechnology Inc., Santa Cruz, CA, USA), Drp1 (C-5) (1 : 1000; Sc-271583, Santa Cruz Biotechnology), phospho-Drp1(Ser616) (1 : 1000; #3455, Cell Signaling Technology Inc., Beverly, MA, USA), Caspase-8 (1C12) (1 : 750; #9746, Cell Signaling Technology), ATPase $\beta$-subunit (1 : 10 000; ab14 730, Abcam plc., Cambridge, UK), GAPDH (glyceraldehyde 3-phosphate dehydrogenase; 1 : 20 000; ab9482, Abcam) and TSPO (1 : 10 000; ab109497, Abcam).

**Immunocytochemistry.** For investigating on Bax recruitment to mitochondria in cells modulated for IF$_1$ expression, at a confluence of ~50%, cells growth on Ø 22 mm borosilicate cover slips were transfected with either IF1-YFP cDNA, IF$_1$ siRNA and YFP cDNA or YFP cDNA (as a control). After 36 h of transfection, apoptosis was induced by treating cells with 1 $\mu$M STS in recording medium (4 h incubation at 37 °C, 5% CO2); as a control, cells were treated with DMSO vehicle. Cells were then washed with warm PBS and fixed with 4% paraformaldehyde in PBS (15 min incubation at RT). Following washes with PBS at RT, cell permeabilization was achieved through incubation with 0.1% Triton X-100 in PBS (30 min at RT). Cells were then washed three times with PBS for 5 min at RT. Background or unspecific staining were avoided using normal goat serum blocking solution (10% normal goat serum, 3% bovine serum albumin in 0.01% Triton X-100 in PBS; 1 h incubation at RT). Cells were incubated in the dark overnight at 4 °C with the primary antibody to Bax (6A7) (sc-23959) at dilution 1 : 200 (in 0.01% Triton X-100 in PBS). After five washes with PBS to remove unbound primary antibodies, Alexa Fluor 555-conjugated secondary antibody to mouse IgG was added at dilution 1 : 1000 (in 0.01% Triton X-100 in PBS; 1 h incubation in the dark at RT). Unbound secondary antibodies were removed by washing cells with PBS five times. Nuclei were stained with 10 $\mu$M TO-PRO®-3 iodide in PBS (20 min incubation in the dark at RT). After five washes with PBS, cover slips were mounted with AF1 mountant solution (Citifluor Ltd., London, UK). Negative controls were performed by omission of primary or secondary antibody. Cells were imaged on a Zeiss LSM 510 Confocal Laser Scanning Microscope (inverted configuration on an Axiovert 200 frame) using a 'Fluar' × 40/1.30 oil immersion objective. To avoid contamination between fluorescent dyes emission, images were acquired in three consecutive scans, using an Argon laser (488 nm line) for YFP, a green Helium-Neon laser (543 nm line) for Alexa Fluor 555 and a red Helium-Neon laser (633 nm line) for TO-PRO-3 iodide. Illumination intensity was kept to a minimum (0.1–2%) to avoid bleaching of the fluorescent signals. Settings were chosen to minimize bleaching. The fluorescence emission of YFP was captured through the HTF 488/514 dichroic mirror with BP 500/550 band pass filter, Alexa Fluor 555 through the HFT 488/543 dichroic mirror with BP 535/590 and TO-PRO-3 through the HTF UV/488/543/633 dichroic mirror with LP 650 high-pass filter. Acquired images were processed with the LSM Image Browser software.

The same procedure was followed for immunocytochemistry analysis of mitochondrial translocation of Drp1. Cells were cotransfected with the mitochondrially targeted red fluorescent protein and a blank vector (control cells), IF$_1$ cDNA ( + IF$_1$ cells) or an siRNA against IF$_1$ ( − IF$_1$ cells). Cells were then treated with STS for 4 h and stained with an anti-Drp1 antibody and an Alexa Fluor 488-conjugated anti-Mouse IgG antibody (Invitrogen; Life Technologies Ltd., Paisley, UK). DAPI was used for nuclear staining.

**Calcineurin activity assay.** At a confluence of ~50%, cells cultured on 100 mm Petri dishes were transfected with IF$_1$ cDNA, IF$_1$ siRNA or an empty vector (as a control). After 36 h of transfection, cells were incubated with 1 $\mu$M STS supplemented medium (4 h incubation at 37 °C, 5% $CO_2$) to induce apoptosis; DMSO vehicle was used as a control. After treatment, Calcineurin activity was measured using a Calcineurin cellular activity assay kit (Enzo Life Sciences Inc., Farmingdale, NY, USA), following manufacturer's instructions.

## Conflict of Interest

The authors declare no conflict of interest.

**Acknowledgements**. Marie Curie Intra-European Fellowship (FP6) for Career Development supported MC at the time the project began. We thank local funds of the RVC for supporting the studentship of DF. Thanks go to BBSRC (New Investigator Award Grant BB/I013695/1), PetPlan Charitable Trust, LAM-Bighi Research Grant on Brain's Tumors, the Association 'il Circolo' for sustaining the experimental activities in MC's laboratory; while MRD thanks the Wellcome Trust. CHT was supported by a UCL graduate school studentship. Special thanks for the enduring key support to Mr Mark Turmaine (UCL Biosciences EM Facility). We are also grateful to Prof. Luca Scorrano (University of Genève) for the generous gift of Drp1-K38A mutant and Drp1$^{-/-}$ mouse embryonic fibroblasts. Thanks go to Mr. Valerio de Biase for helping with the $Ca^{2+}$ experiments, Mrs. Jemma Gatliff, Dr Ramona Lupi for careful reading of the manuscript.

## Author Contributions

MC and MRD designed the study and wrote the paper. DF, CHT, MC and AS performed the experiments.

1. Duchen MR. Roles of mitochondria in health and disease. *Diabetes* 2004; **53**(Suppl 1): S96–102.
2. Green DR, Kroemer G. The pathophysiology of mitochondrial cell death. *Science* 2004; **305**: 626–629.
3. Ballot C, Kluza J, Lancel S, Martoriati A, Hassoun SM, Mortier L *et al.* Inhibition of mitochondrial respiration mediates apoptosis induced by the anti-tumoral alkaloid lamellarin D. *Apoptosis* 2010; **15**: 769–781.
4. Scarlett JL, Sheard PW, Hughes G, Ledgerwood EC, Ku HH, Murphy MP. Changes in mitochondrial membrane potential during staurosporine-induced apoptosis in Jurkat cells. *FEBS Lett* 2000; **475**: 267–272.
5. Rizzuto R, Pozzan T. Microdomains of intracellular Ca2 + : molecular determinants and functional consequences. *Physiol Rev* 2006; **86**: 369–408.
6. Gottlieb E. OPA1 and PARL keep a lid on apoptosis. *Cell* 2006; **126**: 27–29.
7. Pellegrini L, Scorrano L. A cut short to death: Parl and Opa1 in the regulation of mitochondrial morphology and apoptosis. *Cell Death Differ* 2007; **14**: 1275–1284.
8. Fawcett DW. Mitochondria. In: Fawcett WB (ed. *The Cell.* 2nd edn.Philadelphia W. B. Saunders Company, 1981. p 410–478.
9. Rasmussen N. Mitochondrial structure and the practice of cell biology in the 1950s. *J Hist Biol* 1995 Fall **28**: 381–429.
10. Mannella CA, Pfeiffer DR, Bradshaw PC, Moraru II, Slepchenko B, Loew LM *et al.* Topology of the mitochondrial inner membrane: dynamics and bioenergetic implications. *IUBMB Life* 2001; **52**: 93–100.
11. Fulop L, Szanda G, Enyedi B, Varnai P, Spat A. The effect of OPA1 on mitochondrial Ca(2)( + ) signaling. *PLoS One* 2011; **6**: e25199.
12. Mannella CA. The relevance of mitochondrial membrane topology to mitochondrial function. *Biochim Biophys Acta* 2006; **1762**: 140–147.
13. Scorrano L, Ashiya M, Buttle K, Weiler S, Oakes SA, Mannella CA *et al.* A distinct pathway remodels mitochondrial cristae and mobilizes cytochrome c during apoptosis. *Dev Cell* 2002; **2**: 55–67.
14. Faccenda D, Campanella M. Molecular regulation of the mitochondrial F1Fo-ATPsynthase: physiological and pathological significance of the inhibitory factor 1 (IF1). *Int J Cell Biol* 2012; **2012**: 12.
15. Gledhill JR, Montgomery MG, Leslie AG, Walker JE. How the regulatory protein, IF(1), inhibits F(1)-ATPase from bovine mitochondria. *Proc Natl Acad Sci USA* 2007; **104**: 15671–15676.
16. Panchenko MV, Vinogradov AD. Interaction between the mitochondrial ATP synthetase and ATPase inhibitor protein. Active/inactive slow pH-dependent transitions of the inhibitor protein. *FEBS Lett* 1985; **184**: 226–230.
17. Cabezon E, Butler PJ, Runswick MJ, Walker JE. Modulation of the oligomerization state of the bovine F1-ATPase inhibitor protein, IF1, by pH. *J Biol Chem* 2000; **275**: 25460–25464.
18. Cabezon E, Runswick MJ, Leslie AG, Walker JE. The structure of bovine IF(1), the regulatory subunit of mitochondrial F-ATPase. *EMBO J* 2001; **20**: 6990–6996.
19. Campanella M, Casswell E, Chong S, Farah Z, Wieckowski MR, Abramov AY *et al.* Regulation of mitochondrial structure and function by the F1Fo-ATPase inhibitor protein, IF1. *Cell Metab* 2008; **8**: 13–25.
20. Zerbes RM, Bohnert M, Stroud DA, von der Malsburg K, Kram A, Oeljeklaus S *et al.* Role of MINOS in mitochondrial membrane architecture: cristae morphology and outer membrane interactions differentially depend on mitofilin domains. *J Mol Biol* 2012; **422**: 183–191.
21. Strauss M, Hofhaus G, Schroder RR, Kuhlbrandt W. Dimer ribbons of ATP synthase shape the inner mitochondrial membrane. *EMBO J* 2008; **27**: 1154–1160.
22. Garcia JJ, Morales-Rios E, Cortes-Hernandez P, Rodriguez-Zavala JS. The inhibitor protein (IF1) promotes dimerization of the mitochondrial F1F0-ATP synthase. *Biochemistry* 2006; **45**: 12695–12703.
23. Campanella M, Seraphim A, Abeti R, Casswell E, Echave P, Duchen MR. IF1, the endogenous regulator of the F(1)F(o)-ATPsynthase, defines mitochondrial volume fraction in HeLa cells by regulating autophagy. *Biochim Biophys Acta* 2009; **1787**: 393–401.
24. Gomes LC, Di Benedetto G, Scorrano L. During autophagy mitochondria elongate, are spared from degradation and sustain cell viability. *Nat Cell Biol* 2011; **13**: 589–598.
25. Sanchez-Cenizo L, Formentini L, Aldea M, Ortega AD, Garcia-Huerta P, Sanchez-Arago M *et al.* Up-regulation of the ATPase inhibitory factor 1 (IF1) of the mitochondrial H + -ATP synthase in human tumors mediates the metabolic shift of cancer cells to a Warburg phenotype. *J Biol Chem* 2010; **285**: 25308–25313.
26. Domenis R, Comelli M, Bisetto E, Mavelli I. Mitochondrial bioenergetic profile and responses to metabolic inhibition in human hepatocarcinoma cell lines with distinct differentiation characteristics. *J Bioenerg Biomembr* 2011; **43**: 493–505.
27. Formentini L, Sanchez-Arago M, Sanchez-Cenizo L, Cuezva JM. The mitochondrial ATPase inhibitory factor 1 triggers a ROS-mediated retrograde prosurvival and proliferative response. *Mol Cell* 2012; **45**: 731–742.
28. Smirnova E, Griparic L, Shurland DL, van der Bliek AM. Dynamin-related protein Drp1 is required for mitochondrial division in mammalian cells. *Mol Biol Cell* 2001; **12**: 2245–2256.
29. Germain M, Mathai JP, McBride HM, Shore GC. Endoplasmic reticulum BIK initiates DRP1-regulated remodelling of mitochondrial cristae during apoptosis. *EMBO J* 2005; **24**: 1546–1556.
30. Montessuit S, Somasekharan SP, Terrones O, Lucken-Ardjomande S, Herzig S, Schwarzenbacher R *et al.* Membrane remodeling induced by the dynamin-related protein Drp1 stimulates Bax oligomerization. *Cell* 2010; **142**: 889–901.
31. Karbowski M, Lee YJ, Gaume B, Jeong SY, Frank S, Nechushtan A *et al.* Spatial and temporal association of Bax with mitochondrial fission sites, Drp1, and Mfn2 during apoptosis. *J Cell Biol* 2002; **159**: 931–938.
32. Kuwana T, Mackey MR, Perkins G, Ellisman MH, Latterich M, Schneiter R *et al.* Bid, Bax, and lipids cooperate to form supramolecular openings in the outer mitochondrial membrane. *Cell* 2002; **111**: 331–342.
33. Cereghetti GM, Stangherlin A, Martins de Brito O, Chang CR, Blackstone C, Bernardi P *et al.* Dephosphorylation by calcineurin regulates translocation of Drp1 to mitochondria. *Proc Natl Acad Sci USA* 2008; **105**: 15803–15808.
34. Han XJ, Lu YF, Li SA, Kaitsuka T, Sato Y, Tomizawa K *et al.* CaM kinase I alpha-induced phosphorylation of Drp1 regulates mitochondrial morphology. *J Cell Biol* 2008; **182**: 573–585.
35. Pinton P, Rizzuto R. Bcl-2 and Ca2 + homeostasis in the endoplasmic reticulum. *Cell Death Differ* 2006; **13**: 1409–1418.
36. Boehning D, Patterson RL, Sedaghat L, Glebova NO, Kurosaki T, Snyder SH. Cytochrome c binds to inositol (1,4,5) trisphosphate receptors, amplifying calcium-dependent apoptosis. *Nat Cell Biol* 2003; **5**: 1051–1061.
37. Boehning D, Patterson RL, Snyder SH. Apoptosis and calcium: new roles for cytochrome c and inositol 1,4,5-trisphosphate. *Cell Cycle* 2004; **3**: 252–254.
38. Goldstein JC, Waterhouse NJ, Juin P, Evan GI, Green DR. The coordinate release of cytochrome c during apoptosis is rapid, complete and kinetically invariant. *Nat Cell Biol* 2000; **2**: 156–162.
39. Chae HJ, Kang JS, Byun JO, Han KS, Kim DU, Oh SM *et al.* Molecular mechanism of staurosporine-induced apoptosis in osteoblasts. *Pharmacol Res* 2000; **42**: 373–381.
40. Garrido C, Galluzzi L, Brunet M, Puig PE, Didelot C, Kroemer G. Mechanisms of cytochrome c release from mitochondria. *Cell Death Differ* 2006; **13**: 1423–1433.
41. Broekemeier KM, Dempsey ME, Pfeiffer DR. Cyclosporin A is a potent inhibitor of the inner membrane permeability transition in liver mitochondria. *J Biol Chem* 1989; **264**: 7826–7830.
42. Strasser A, O'Connor L, Dixit VM. Apoptosis signaling. *Annu Rev Biochem* 2000; **69**: 217–245.
43. Wolter KG, Hsu YT, Smith CL, Nechushtan A, Xi XG, Youle RJ. Movement of Bax from the cytosol to mitochondria during apoptosis. *J Cell Biol* 1997; **139**: 1281–1292.
44. Otera H, Mihara K. Mitochondrial dynamics: functional link with apoptosis. *Int J Cell Biol* 2012; **2012**: 821676.
45. Frezza C, Cipolat S, Martins de Brito O, Micaroni M, Beznoussenko GV, Rudka T *et al.* OPA1 controls apoptotic cristae remodeling independently from mitochondrial fusion. *Cell* 2006; **126**: 177–189.
46. Li H, Zhu H, Xu CJ, Yuan J. Cleavage of BID by caspase 8 mediates the mitochondrial damage in the Fas pathway of apoptosis. *Cell* 1998; **94**: 491–501.
47. Rouslin W. Regulation of the mitochondrial ATPase in situ in cardiac muscle: role of the inhibitor subunit. *J Bioenerg Biomembr* 1991; **23**: 873–888.
48. Raisova M, Hossini AM, Eberle J, Riebeling C, Wieder T, Sturm I *et al.* The Bax/Bcl-2 ratio determines the susceptibility of human melanoma cells to CD95/Fas-mediated apoptosis. *J Invest Dermatol* 2001; **117**: 333–340.
49. Edlich F, Banerjee S, Suzuki M, Cleland MM, Arnoult D, Wang C *et al.* Bcl-x(L) retrotranslocates Bax from the mitochondria into the cytosol. *Cell* 2011; **145**: 104–116.
50. James DI, Parone PA, Mattenberger Y, Martinou JC. hFis1, a novel component of the mammalian mitochondrial fission machinery. *J Biol Chem* 2003; **278**: 36373–36379.
51. Baumgartner HK, Gerasimenko JV, Thorne C, Ferdek P, Pozzan T, Tepikin AV *et al.* Calcium elevation in mitochondria is the main Ca2 + requirement for mitochondrial permeability transition pore (mPTP) opening. *J Biol Chem* 2009; **284**: 20796–20803.
52. Cribbs JT, Strack S. Reversible phosphorylation of Drp1 by cyclic AMP-dependent protein kinase and calcineurin regulates mitochondrial fission and cell death. *EMBO Rep* 2007; **8**: 939–944.



Supplementary Information accompanies the paper on Cell Death and Differentiation website (http://www.nature.com/cdd)